Magnesium Technology 2013
Edited by: Norbert Hort, Suveen N. Mathaudhu, Neale R. Neelameggham, and Martyn Alderman
TMS (The Minerals, Metals & Materials Society), 2013

A new magnesium alloy system: TEXAS

Björn Wiese[1], Chamini Mendis[1], Carsten Blawert[1], Eric Nyberg[2], Karl Ulrich Kainer[1], Norbert Hort[1]
[1]MagIC-Magnesium Innovation Center, Helmholtz-Zentrum Geesthacht, Max-Planck-Straße 1, D-21502 Geesthacht, Germany
[2]Pacific Northwest National Laboratory, 902 Battelle Boulevard, Richland, WA, USA

Keywords: magnesium alloy system, MgCaSn phase, microstructure, mechanical properties, corrosion

Abstract

A new TEXAS alloy system (Mg-Sn-Nd-Ca-Al-Si) is presented in order to extend the range of applications for magnesium alloys. The alloy has been produced by permanent mould direct chill casting, a process that provides a homogenous distribution of alloying elements throughout the entire casting. This work presents microstructural features and a new Mg-Sn-Ca phase with the morphology of hexagonal platelets. Additionally mechanical properties and the corrosion behaviour of TEXAS alloys are presented in as cast and heat treated conditions.

Introduction

Magnesium (Mg) alloys have low density and are used in automobile and aerospace applications where lightweight is of importance. Mg-Sn-Ca (TX) alloys has been developed as creep resistant alloys [1]. In this system Sn forms solid solution with Mg to provide corrosion resistance while Ca forms intermetallic particles in the matrix. The alloys based on this system, have tensile yield strengths similar to AZ31 alloy, commercially available Mg alloy with good combination of strength and corrosion resistance.

The new magnesium alloys, TEXAS, are based on the Mg-Sn-Nd-Ca-Al-Si system and are expected to extend the range of the applications possible for the TX system [1, 2, 3, 4, 5, 6, 7, 8, 9]. The first steps in extending the TX system were based on investigations into TXAS, TXA and TXS form [10]. Formation new phases, the increase the mechanical properties at the room temperature and at elevated temperatures was expected with Si and Al addition [11]. Studies on the influence of rare earth elements such as Ce, Zr and Gd, on the Mg3Sn2Ca (TX32) alloys were already investigated [12, 13, 14, 15].

This paper is the first step to investigate microstructure, mechanical properties and corrosion resistance of this TEXAS alloy system. Here we report the microstructure characterisation of the as cast alloys. The mechanical properties and corrosion resistance of the as cast (F) and the T4 heat treated alloys are also reported in this contribution.

Experimental Procedure

Pure Mg (99.99 %, Hydro Magnesium), pure Sn (99.995 %, ChemPur), pure Nd (99.5 %, Griem Ad- vanced Material co., Ltd), pure Al (99.99 %), pure Si (99.9 %, ChemPur) and pure Ca (99 %, Alfa Aesar) melted in a mild steel crucible to produce alloys with 3.0 wt% Sn, 0.3 wt% Nd, 0.3 wt% Al, 0.3 wt% Si and varying amounts of Ca from 0.5 wt% to 2.0 wt%. All alloys have been prepared by permanent mould direct chill casting, because this is a special method of casting [16]. Alloys were melted in flowing Ar+3 % SF6 in an induction furnace (Nabertherm, Germany) at a temperature of 720 °C and Sn, Nd, Ca, Al and Si were added to the magnesium melt. The melt was kept for five minutes without stirring and was poured into a permanent steel mold (55 x 110 x 270 mm) which was preheated to 350 °C. The melt was kept for 15 min at 680 °C. The cast ingots were cooled down to room temperature by water quenching as reported elsewhere [16]. Table 1 list the nominal composition of the alloys investigated. The specimens were solution heat treated at 500 °C for 6 h and cooled down to room temperature by water quenching (T4 condition).

Table 1: Nominal composition of the TEXAS alloys (wt%)

alloy	Compositions (wt%)					
	Sn	Nd	Ca	Al	Si	Mg
TEXAS A	3	1.5	2.0	0.3	0.3	bal
TEXAS B	3	1.5	1.0	0.3	0.3	bal
TEXAS C	3	1.5	0.5	0.3	0.3	bal

The specimens for scanning electron microscopy (SEM) were prepared by grinding with SiC paper to 2500 grit, and then polished with, 3 µm diamond paste followed by a mixture of 1 µm diamond suspension and OPS™ anhydrous suspension. Microstructures were investigated using a ZEISS, ULTRAT M 55 SEM equipped with an EDAX energy-dispersive X-ray spectrometer (EDXS) and local compositions determined by point analysis. The specimens of 5 x 20 x 30 mm were ground down to a 2500 grit SiC paper, polished with 1 µm OPST M anhydrous suspension and then cleaned with ethanol and dried are used for X-ray diffraction (XRD). The phase identification was carried out with a X´Pert PRO PANalytical and HighScorePlus XRD operating at 40 kV and 40 mA with Cu Kα (wavelength λ = 0.15406 nm) radiation. The measurements were conducted by scanning (2Θ) from 15° to 100° with a step size of 0.025°. A acquisition time of 2 s per step was used.

Tensile tests were conducted in accordance to DIN EN 10002 and DIN 50106 at room temperature using a Zwick 050 testing machine (Zwick GmbH & Co., KG). An initial strain rate of 0.001 s^{-1} in was used. The Vickers hardness was measured using a EMCO-TEST the M1C 010, indenter with a 5 kg load and the value reported is the average from 10 measurements per sample. The specimens for hardness measurement were ground to a 2500 grit SiC finish.

Potentio-dynamic polarisation measurements were performed in 0.5 % NaCl solution. A starting pH value of 7 was adjusted with

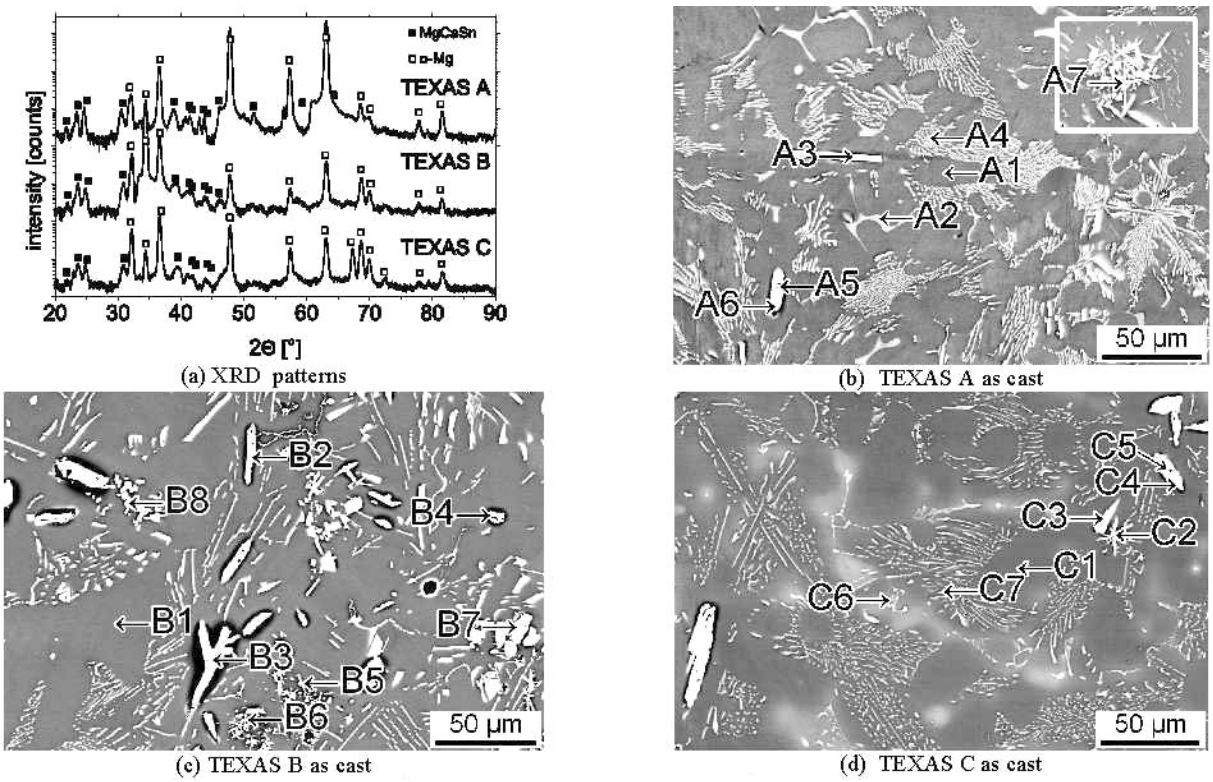

(a) XRD patterns (b) TEXAS A as cast

(c) TEXAS B as cast (d) TEXAS C as cast

Figure 1: (a) XRD patterns and (b,c,d) SEM Backscattered Electrons (BSE) microstructure of TEXAS alloys.

Table 2: EDX of striking points from TEXAS A, B and C to the Figure 1.

Alloys	Compositions at%									
	points	Mg	Al	Si	Sn	Ca	Nd	Mg/(Sn+Ca)	Si/Nd	Sn/Ca
TEXAS A	A1	99.7	0.0	0.0	0.1	0.1	0.0	-	-	-
	A2	94.7	0.0	0.9	1.9	2.4	0.2	-	-	0.8
	A3	86.7	2.1	0.0	0.1	10.9	0.2	7.9		0.0
	A4	49.1	0.0	4.8	22.5	21.8	1.8	1.1	2.7	1.0
	A5	67.0	0.4	5.0	13.3	12.9	1.3	2.6	3.7	1.0
	A6	41.0	0.0	5.5	25.8	24.3	3.4	0.8	1.6	1.1
	A7	23.9	0.0	34.7	0.8	1.1	39.1	-	0.9	-
TEXAS B	B1	99.7	0.0	0.0	0.2	0.1	0.0	-	-	-
	B2	42.2	0.1	7.9	22.7	25.4	1.7	0.9	4.6	0.9
	B3	54.9	0.1	6.0	17.9	19.8	1.4	1.5	4.3	0.9
	B4	35.9	0.0	8.1	25.1	29.0	1.9	0.7	4.2	0.9
	B5	68.3	0.1	15.6	0.1	0.3	15.6	-	1.0	-
	B6	65.6	0.0	17.4	0.2	0.4	16.5	-	1.1	-
	B7	25.9	1.4	32.1	1.7	0.1	38.9	-	0.8	-
	B8	35.8	0.0	31.0	0.6	0.6	32.0	-	1.0	-
TEXAS C	C1	99.7	0.0	0.1	0.2	0.1	0.0	-	-	-
	C2	37.4	0.0	29.0	1.8	5.1	26.8	-	1.1	-
	C3	41.3	0.0	11.8	19.8	24.9	2.2	0.9	5.3	0.8
	C4	35.6	0.0	11.6	21.6	28.5	2.8	0.7	4.2	0.8
	C5	58.7	0.1	4.7	15.7	20.2	0.7	1.6	6.8	0.8
	C6	76.9	0.0	20.1	2.8	0.2	0.0	-	-	14.8
	C7	92.2	0.0	2.2	2.2	3.4	0.2	16.8	14.4	0.6

NaOH. The measurements were performed in a standard three electrode set-up with the alloy specimens as working electrodes (1.54 cm2 area in contact with the electrolyte) in conjunction with an Ag/AgCl reference electrode and a platinum counter electrode. After 30 min the free corrosion potential were recorded, the polarisation scan was measured with a scan rate of 0.2 mV s^{-1}. The test completed at a corrosion current of 10 mA. The corrosion rate was determined from the cathodic component of the corrosion curve.

Results and Discussion

Microstructure and Phase Characterization

The XRD patterns of as cast TEXAS A, B and C are shown in Figure 1(a). The XRD shows the presence of Mg and MgCaSn phase (orthorhombic phase) and no phase containing Nd or Si were detected. The investigations by SEM and EDX showed in addition to a phase containing Mg, Ca and Sn number of phases containing Mg, Ca, Si, Nd and another phase with Nd and Si. These phases are not found in the XRD measurement as the volume fraction of these phases are likely to be lower than the detection limit of XRD and need to be investigated by TEM. The SEM microstructures of the three TEXAS alloys A, B and C shown in Figures 1 with EDX measurement are listed in Table 2.

Dendritic microstructures were observed in all three alloys, with hexagonal platelets of MgCaSn phase similar to that observed in the TX alloys [1, 2]. The hexagonal shape of these precipitates varies with Ca content of the alloy and they show a more irregular hexagonal shape reduction of Ca. The platelets (Figure 1(b) to 1(d)) show dark points in the centre and the EDX measurements give a higher Mg composition at the centre compared to the areas away from these points (Point A5 and C5 in the centre and A6 and C4 in the platelets). The Mg-rich areas in the centre of plates are expected to act as a nucleus for the formation of the MgCaSn phase. The composition of the platelets are similar to that reported previously [1, 2, 3, 4] with a ratio of Sn to Ca of 0.8 to 1.0 in the ternary phase CaMgSn which decreases with the decreases in Ca concentration. However, the eutectic areas showed a comparable ratio of Sn to Ca. The stoichiometric ratio between Sn:Ca changed in this alloy system in TEXAS A 1:2, in TEXAS B 1:1 and in TEXAS C 2:1. The TEXAS A and B alloys can bind the entire Ca with Sn in the MgCaSn phases. In TEXAS C Mg_2Sn and in TEXAS A Mg_2Ca are also likely to form as in the TX system [6]. The XRD patterns do not shows the Mg_2Sn and Mg_2Ca phases Figure 1(a).

In TX alloys with the addition of RE no RE containing particles were detected [13, 14, 15], In this case Nd and as well Si was formed in the platelets but such phases are yet to be characterised. The Nd and Si leads to needle-shaped precipitates as shown by SEM-EDX Figure 1 on the points A7, B5, B6 and C2. The ratio between Nd and Si is approximately 1 in all alloys. The detection of the Nd-Si precipitates by XRD was not possible.

Another phase that is observed in the TEXAS C contained of Mg and Si (point C6). The formation of Mg-Si phase appears to be suppressed by the Ca concentration in TEXAS A and B but with the reduction of Ca content Mg-Si phase also forms. Additions of Ca changed the microstructure and caused a morphological change the characteristic shape of Mg_2Si Chinese Script particles from sharp needle like particles to more curved particles. The modification mechanism of Ca is polygonal type Mg_2Si particles nucleating from $CaSi_2$ particles has been reported previously [17]. Again the XRD analysis do not show the Mg_2Si phase.

Mechanical Properties

Table 3 list the hardness of the three TEXAS alloys in the as cast (F) and the T4 heat treated conditions. The TEXAS A alloy with the highest Ca concentration shows the highest hardness value in each condition. The alloys TEXAS B and C with the lower Ca concentration show similar to hardness values in the as cast and the T4 heat treated conditions. The heat T4 treatment did not reduce the hardness of any TEXAS alloys and any reductions were within the standard deviation of the measurements. The reduction in the Ca concentration from 2 to 1 wt % reduced the hardness, as less of Ca-rich phases are present in the microstructure.

Table 3: Mechanical properties like TYS, UTS, A and hardness for the TEXAS alloys in as cast (F) and T4 heat treated conditions.

	cond.	TEXAS		
		A	B	C
TYS [MPa]	F	79.69 ± 3.60	66.78 ± 1.56	70.52 ± 0.18
	T4	62.39 ± 1.62	56.03 ± 1.39	61.78 ± 3.80
UTS [MPa]	F	113.64 ± 3.12	108.46 ± 13.29	125.56 ± 3.77
	T4	99.42 ± 4.48	104.45 ± 7.15	117.36 ± 2.30
A [%]	F	1.16 ± 0.12	1.45 ± 0.54	2.59 ± 0.21
	T4	1.54 ± 0.28	2.03 ± 0.37	2.61 ± 0.57
hardness [HV]	F	47.91 ± 3.04	41.69 ± 3.81	41.78 ± 3.18
	T4	46.29 ± 3.72	39.52 ± 2.86	37.59 ± 4.07

The Table 3 and the Figures show the tensile properties of alloys tested in the as cast (F) and the T4 heat treated conditions. In comparison with the as cast condition, the T4 condition show a decrease in the tensile yield strength (TYS) and ultimate tensile strength (UTS) for all alloys but with an increase in the elongation (A) for TEXAS A and B. The decrement of the UTS does not show such a clear trend after T4. The T4 heat treatment has the biggest influence on the TYS a decrease 80 to 62 MPa in TEXAS A. TEXAS B shows the highest increase of the elongation (A) after T4. The highest ductility was observed in the T4 heat treated TEXAS C alloy. The Ca content has a major influence on the strength where higher the Ca content higher the TYS.

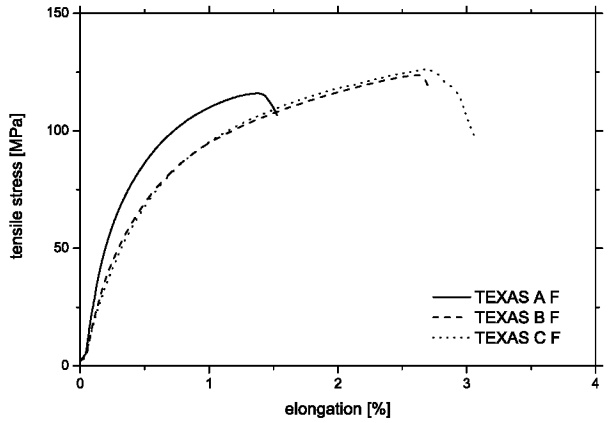

(a)

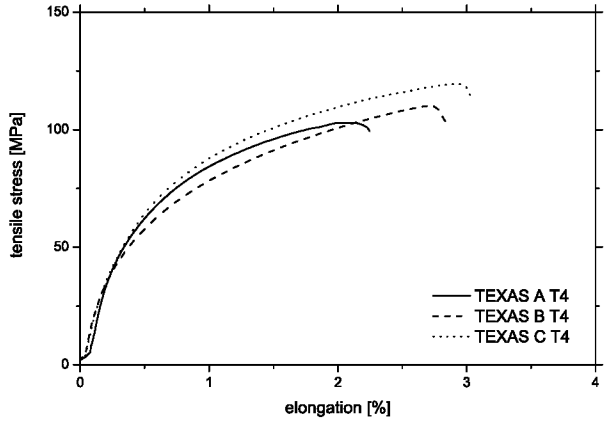

(b)

Figure 2: Load-deformation curves of TEXAS A, B and C (a) in as cast (F) and (b) T4 heat treated conditions.

Corrosion Properties

The results from the potentio-dynamic polarisation measurements are listed in Table 4. All three alloys are similar and show filiform corrosion on the surface and deep holes in the shape of hexagonal platelets. These particles probably act as a galvanic site and are the starting points for corrosion. The EDX measurements showed that this platelets are phases rich of Sn, Ca and Mg and the corrosion rate is dependent on the Ca and Sn concentration. The cast TEXAS A, with the highest Ca concentration, shows the maximum corrosion rate.

After the T4 heat treatment, the corrosion at TEXAS A is apparently lower, as the microstructure has been homogenized and some of the Mg,Ca,Sn phase has gone into solution. The corrosion rate of TEXAS B after T4 heat treatment is similar to that of the as cast condition. However, the corrosion rate increases after T4 heat treatment of the TEXAS C alloys, likely due to the precipitates, probably Sn phase is dissolved in preference to the Ca, Sn containing phase.

Table 4: Polarisation measurements for the TEXAS alloys.

TEXAS	cond.	Free corr Potential [mV]	Icorr [mA]	Corrosion-Rate [mm/a]
A	F	-1564.0 ± 1.0	0.253 ± 0.036	3.75 ± 0.53
	T4	-1568.3 ± 1.2	0.179 ± 0.019	2.66 ± 0.28
B	F	-1552.3 ± 0.6	0.132 ± 0.034	1.96 ± 0.51
	T4	-1555.7 ± 0.6	0.122 ± 0.029	1.82 ± 0.42
C	F	-1577.0 ± 20.0	0.121 ± 0.017	1.80 ± 0.25
	T4	-1575.3 ± 4.9	0.158 ± 0.006	2.34 ± 0.09

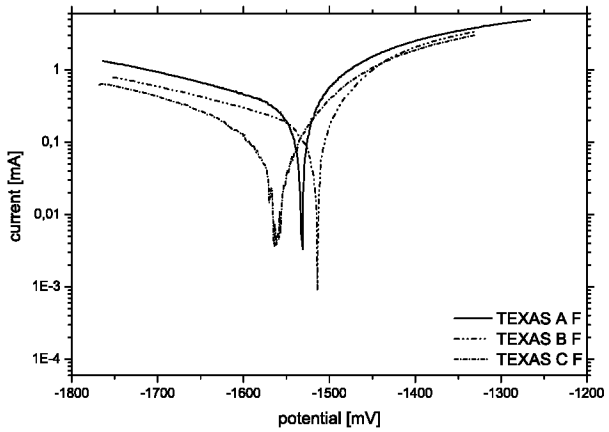

(a)

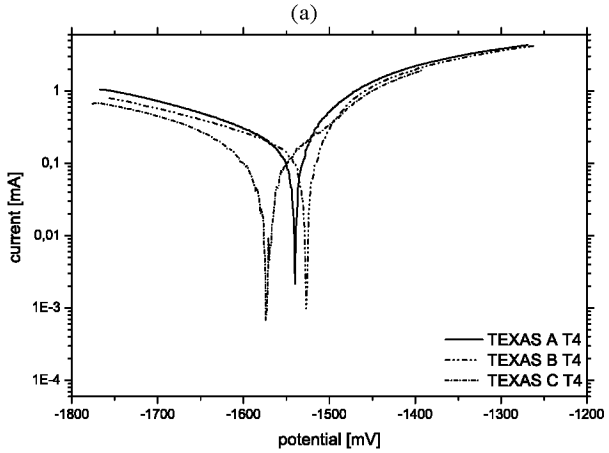

(b)

Figure 3: Typical experimental polarisation curves for corrosion resistance of TEXAS A increases, TEXAS B remains similar to the as cast condition and TEXAS C decreases.

Conclusions

1) The variation of the Ca content of between 0.5 and 2.0 wt% has a strong influence on the microstructure of the as cast TEXAS alloys. The hexagonal shape of the MgCaSn platelets can be seen clearly with increasing Ca content. With the lowest Ca content of 0.5 wt% was Mg-Si phase was observed. All three alloys show needle-shaped Nd-Si precipitates but are not observed with XRD.

2) The increase in Ca content reduces the ductility in the TEXAS alloys and leads to an increase in tensile yield strength. The ductility of TEXAS alloy system rather low, with maximum elongation of 2.6 % measured for the TEXAS C containing lowest content of Ca.

3) The corrosion resistance of the three alloys are different in the as cast and the T4 heat treated conditions. With a lower Ca concentration in the TEXAS alloys show a decrease in the corrosion rate in the as cast condition. After the T4 heat treatment the corrosion resistance of TEXAS A increases, TEXAS B remains similar to the as cast condition and TEXAS C decreases.

References

[1] T. Abu Leil et al. "Microstructure, corrosion and creep of as-cast magnesium alloys," In R.S. Beals, M.O. Pekguleryuz, R. Neelameggham, and A.A. Luo, editors, *TMS Magnesium Technology* (2007).

[2] N. Hort et al. "Microstructural Investigations of the Mg-Sn-xCa System," *Advanced Engineering Materials*, 8 (2006), 359–364.

[3] A. Kozlov et al. "Phase equilibria, thermodynamics and solidification microstructures of Mg-Sn-Ca alloys, Part 1: Experimental investigation and thermodynamic modeling of the ternary Mg-Sn-Ca system," *Intermetallics*, 16 (2008), 299–315.

[4] A. Kozlov et al. "Phase equilibria, thermodynamics and solidification microstructures of Mg-Sn-Ca alloys, Part 2: Prediction of phase formation in Mg-rich Mg-Sn-Ca cast alloys," *Intermetallics*, 16 (2008), 316–321.

[5] K.P. Rao et al. "Hot workability characteristics of cast and homogenized Mg-3Sn-1Ca alloy," *Journal of Materials Processing Technology*, 201 (2008), 359–363.

[6] T. Abu Leil et al. "Microstructure and corrosion behavior of Mg-Sn-Ca alloys after extrusion," *Transactions of Nonferrous Metals Society of China*, 19 (2009), 40–44.

[7] Y.V.R.K. Prasad et al. "Hot working parameters and mechanisms in as-cast Mg-3Sn-1Ca alloy," *Materials Letters*, 62 (2008), 4207–4209.

[8] M. Yang, L. Cheng, and F. Pan. "Comparison of as-cast microstructure, tensile and creep properties for Mg-3Sn-1Ca and Mg-3Sn-2Ca magnesium alloys," *Transactions of Nonferrous Metals Society of China*, 20 (2010), 584–589.

[9] G.H. Hasani and R. Mahmudi. "Tensile properties of hot rolled Mg-3Sn-1Ca alloy sheets at elevated temperatures," *Materials and Design*, 32 (2011), 3736–3741.

[10] K.P. Rao et al. "Effect of Minor Additions of Al and Si on the Mechanical Properties of Cast Mg-3Sn-2Ca Alloys in Low Temperature Range," *Materials Science Forum*, 654-656 (2010), 635–638.

[11] N. Hort, Y. Huang, and K. U. Kainer. "Intermetallics in Magnesium Alloys," *Advanced Engineering Materials*, 8 (2006), 235–240.

[12] B. Shi, R. Chen, and W. Ke. "Effect of element Gd on phase constituent and mechanical property of Mg-5Sn-1Ca alloy," *Transactions of Nonferrous Metals Society of China*, 20 (2010), 341–345.

[13] M. Yang et al. "Effects of zirconium addition on as-cast microstructure and mechanical properties of Mg-3Sn-2Ca magnesium alloy," *Materials and Design*, 32 (2011), 1967–1973.

[14] M. Yang, Y. Ma, and F. Pan. "Effects of little Ce addition on as-cast microstructure and creep properties of Mg-3Sn-2Ca magnesium alloy," *Transactions of Nonferrous Metals Society of China*, 19 (2009), 1087–1092.